Rheological evaluation of the fabrication parameters of cellulose acetate butyrate membrane on CO_2/N_2 separation performance

R J Lee[1], Z A Jawad[1]*, A L Ahmad[2], H B Chua[1], H P Ngang[2], S H S Zein[3]

[1] School of Engineering and Science, Department of Chemical Engineering, Curtin University Malaysia, CDT 250, Miri 98009, Sarawak, Malaysia

[2] School of Chemical Engineering, Engineering Campus, Universities Sains Malaysia, 14300 Nibong Tebal, Penang, Malaysia

[3] Chemical Engineering, School of Engineering and Computer Science, University of Hull, Hull, HU6 7RX, United Kingdom.

*Corresponding author: zeinab.aj@curtin.edu.my

Tel: +60 85 443939 (2414), Fax: +60 85 443837

This is the accepted manuscript of a book chapter published in Jawad, Z. (Ed.). (2019). Membrane Technology for CO2 Sequestration. Boca Raton: CRC Press, https://doi.org/10.1201/b22409

Abstract

The rise in emission of greenhouse gases (GHGs) mainly carbon dioxide (CO_2) in recent years due to rapid development of modern civilisation, has been listed as the primary contributor to global warming. To address this global issue, membrane technology was applied and developed intensively because of its superior performance in terms of efficiency and economic advantages. In this study, the cellulose acetate butyrate (CAB) polymer was selected as the polymer matrix material since it exhibited excellent film-forming properties. In addition, the wet-phase inversion technique was adopted to synthesise the membrane based on different casting conditions. The optimum outcomes of the fabrication conditions were then characterised with the scanning electron micrograph (SEM) to determine the best CAB membrane for CO_2/N_2 separation. The results showed that CAB-70000 fabricated with 4 wt% of CAB polymer concentration, casting thickness of 250 µm, solvent evaporation time of 5 minutes, and 30 minutes of solvent exchange for isopropyl alcohol and n-hexane, exhibited the best gas separation performance. Further, CAB-70000 showed an average selectivity of 6.12 ± 0.09 and permeance up to 227.95 ± 0.39 GPU for CO_2 and 37.28 ± 0.54 GPU for N_2, respectively. In summary, this study is expected to show a detailed outline of the future direction and perspective of the novel CAB polymeric membrane that is suitable to be applied in the industry, and serves as an insight for researchers and manufacturers working in the related field of gas separation.

1.0 Introduction

There is a trend of rapid increase in world population, which is expected to hit 10 billion by 2050 (Lalia et al., 2013). In this regard, higher demand in energy will be required for the 21st century to meet the urgent needs. It is predicted that the energy demand will increase by 57 per cent in 2030 (Conti et al., 2016). As a major contributor to the world energy supply, fossil fuel solely contribute around 40 per cent of the total carbon dioxide (CO_2) emission into the environment, which is mainly attributed to the massive coal combustion activities (Carapellucci and Milazzo, 2003). Global warming has become a genuine problem due to the excessive discharge of pollutants emitted from the combustion activities in the primary industries (Yang et al., 2008).

In the past few decades through their efforts, researchers have contributed in combating this global issue to limit and minimise the impact of greenhouse gases (GHGs). They have outlined three feasible options. The first comprises of saving energy used intensively with methods that are more efficient. The second option is to minimise the usage of carbon-based material source or replace it with renewable energy, and the third is to improve the effectiveness of CO_2 sequestration with more advanced technology development (Yang et al., 2008). For the past few years, membrane separation technology has been utilised intensively for both water treatment and gas separation purpose (Yang et al., 2008, Kappel et al., 2014, Barnes et al., 2014, Zhu et al., 2014). The membrane's chemical and physical properties, and interaction between permeance and membrane are relatively crucial factors in determining the diffusion characteristics of the gas separation field (Shekhawat, 2003). This is because the separation selectivity and permeance are two critical parameters that indicate membrane separation performance. In an ideal situation, high selectivity and permeance are preferred as both induce less capital costs and operating expenses for the industries (Paradise and Goswami, 2007, Low et al., 2013). Hence, the selection of material plays an influential role, in determining the specific gas separation performance (Lalia et al., 2013, Zha et al., 2015, Feng et al., 2015).

The cellulose acetate butyrate (CAB) possesses few interesting characteristics that include, film-forming properties, acetyl and butyryl functional groups, which can effectively improve and further expand the capacity of cellulose chain giving high sorption characteristic, as well as high impact,

weather and chemical resistant (Feng et al., 2015, Basu et al., 2010, Kunthadong et al., 2015). The CAB was first investigated and studied by Sourirajan back in 1958, then followed by Manjikian and others in reverse osmosis (RO) separation (Wang et al., 1994). They reported that the CAB membrane owned high solute separation with tolerable membrane flux result, and also provided ease of fabrication as some pre-treatment was negligible (Ohya et al., 1980, Wang et al., 1994). However, limited studies have been conducted on the effects of the acetyl group content on CAB membranes in the CO_2/N_2 gas separation field. Further, no reports or systematic studies have been performed on the effects of membrane production procedure and fabrication parameters. This includes membrane-casting thickness, solvent exchange time for both isopropyl alcohol and n-hexane with different CAB molecular weights as well as the polymer matrix material structure and performance of CAB membranes. Therefore, the primary objective of this study is to investigate the effects of membrane production procedure and fabrication parameters. Discussions on how the mentioned parameters can affect the membrane in terms of morphology and gas separation performance are presented in this report. The separation performance of the synthesised CAB membrane was selected to evaluate the specified parameters towards CO_2/N_2.

2.0 Methodology

2.1 Materials

The cellulose acetate butyrate (CAB, M_n~12000, 65000, 70000) in powder form was purchased from Sigma-Aldrich (Malaysia) for membrane preparation. Solutions required for membrane preparation i.e., chloroform, isopropyl alcohol, and n-hexane were purchased from Merck (Malaysia). Distilled water was used for the phase-inversion steps, specifically for immersion precipitation for membrane formation.

2.2 CAB Polymer dope preparation

The CAB membrane was prepared using the wet-phase inversion method, followed by solvent exchange to dry the membrane. A dope solution consisting of 4 wt% CAB (*Mn*=70000) powders and 96 wt% chloroform was prepared following the condition of each parameter. The solution was stirred for 24 hours, and then sonicated for 20 minutes to eliminate the gas bubbles in the solution (Ahmad et al., 2014, Feng et al., 2015). The solution was then poured into space within the casting bars with glass plate

underneath. An automatic film applicator (Elcometer 4340, E.U.) was then used for the casting of the membrane. Referring to our previous work, 5 minutes of solvent evaporation time was allowed following each parameter's condition before immersing the membrane in distilled water (27 °C) for a duration of 24 hours (S.Minhas, 1992, Lee et al., 2017). The solvent exchange was performed on the as-spun membrane first with 60 minutes immersion period in isopropyl alcohol and then another 60 minutes immersion period in n-hexane. The resultant membrane was then dried at ambient temperature to eliminate the remaining volatile liquid in between two glass plates filled with filter paper for 24 hours before use (S.Minhas, 1992, Jawad et al., 2015a)

2.2.1 Effect of casting thickness

The membranes were prepared at different casting thicknesses following the fabrication method as described in section 2.2 where the study range for this parameter was from 200 µm (CAB-200), 250 µm (CAB-250) to 300 µm (CAB-300).

2.2.2 Effect of exchange time with isopropyl alcohol

Meanwhile, for the effect of solvent exchange time, the membranes were prepared following the fabrication method as described in section 2.2. The solvent exchange duration studied was 15 minutes (CAB-15Iso), 30 minutes (CAB-30Iso), and 60 minutes (CAB-60Iso) for isopropyl alcohol, followed by 60 minutes of n-hexane.

2.2.3 Effect of exchange time with n-hexane

In addition, the solution of the solvent exchange time with n-hexane was prepared following the fabrication method as described in section 2.2. The resultant membranes were first solvent exchanged with isopropyl alcohol for 30 minutes followed by solvent exchange times ranging from 15 minutes (CAB-15H), 30 minutes (CAB-30H) to 60 minutes (CAB-60H) for n-hexane.

2.2.4 Effect of CAB at different molecular weight (M_n)

The membranes were prepared with different CAB molecular weights (M_n) of 12000 (CAB-12000), 65000 (CAB-65000), and 70000 (CAB-70000) for the preparation of the dope solution. After that, following the fabrication method as mentioned in section 2.2, the solvent exchange time for isopropyl alcohol and n-hexane were set for 30 minutes each.

2.3 Membrane permeability test

The procedure for gas permeation measurement was discussed in our previous published work (Lee et al., 2017).

2.4 Membrane characterization

2.4.1 Scanning Electron Microscopy (SEM)

The CAB membrane structures including surface and cross-sectional, were observed via SEM (Hitachi TM3000, Tokyo, Japan). Each membrane sample was cut into small pieces, and then kept on a plastic petri dish in the cryogenic freezer at a temperature of up to -80°C for 24 hours to give a consistent and clean-cut by freezing. The samples were coated with a platinum layer to prevent high-energy beam damage before the characterisation works. Further, each sample's average membrane thickness was calculated based on the frequency count as measured by the Image-J software. Approximately, 100 measurements were taken to confirm the average membrane thickness.

2.4.2 X-ray Photoelectron Spectroscopy (XPS)

The CAB membranes fabricated at different molecular weights were characterised with the High Resolution Multi-Technique X-Ray Spectrometer (Axis Ultra DLD XPS, Kratos, Shimadzu Corporation, Japan). The analysis was carried out using a PHI 1600 spectrometer with hybrid lens mode, 150 W (Anode: Mono), 1000 meV step, and 5 sweeps for each membrane at room temperature.

3.0 Results and Discussion

3.1 Effect of casting thickness

The effect of casting thickness on the structure and performance of the CAB membrane was investigated, as depicted in **Fig. 1**. As observed from **Fig. 1a**, the structure of CAB-200 (200 µm) was porous. As the casting thickness of the membranes increased, a smooth surface was observed for CAB-250 (250 µm), as demonstrated in **Fig. 1c**. Alternatively, a rough surface was formed for CAB-300 (250 µm), as seen in **Fig. 1e.** The change in the structure was due to the different rates of demixing that occurred as the phase precipitation proceeded when high casting thickness was applied, causing the deposition speed of the membrane to reduce during the membrane formation phase. The slow deposition rate avoids rapid

exchange of non-solvent and solvent within the membrane. As a result, the surface structure of the CAB membrane was built-up based on the sufficient phase precipitation period given (Ahmad et al., 2013, Thomas et al., 2014).

The cross-sectional micrographs of the fabricated CAB membrane at casting thickness of 200 µm (CAB-200), 250 µm (CAB-250), and 300 µm (CAB-300) were revealed in **Figs. 1b**, **d**, and **f**, respectively. From the micrographs, dense structures were depicted from all the cross-sectionals of the CAB membranes. The dense structure formation was due to the densification of the membrane during the immersion period, whereby the remaining solvent imbedded in the polymer matrix was replaced by distilled water. As the volatility of the solvent was generally higher than distilled water the membrane thickness changed from 12.42 ± 0.05 µm to 11.32 ± 0.06 µm and 12.89 ± 0.10 µm for CAB-200, CAB-250 and CAB-300, respectively. The reduction of membrane thickness from 12.42 ± 0.05 µm (CAB-200) to 11.32 ± 0.06 µm (CAB-250) was due to thicker casting thickness applied during membrane fabrication, which allows more solvent embedded in the polymer matrix to be replaced by non-solvent (H_20) during the immersion period, resulting in a denser and thinner membrane thickness for CAB-250 (Ahmad et al., 2013). In contrast, a thicker membrane was obtained when increasing the membrane thickness further to 300 µm for CAB-300 (12.89 ± 0.10 µm). This is correlated to the increase resistance of inward diffusion of non-solvent, due to higher casting thickness applied, causing a delay transition demixing in the film membrane (Tiraferri et al., 2011).

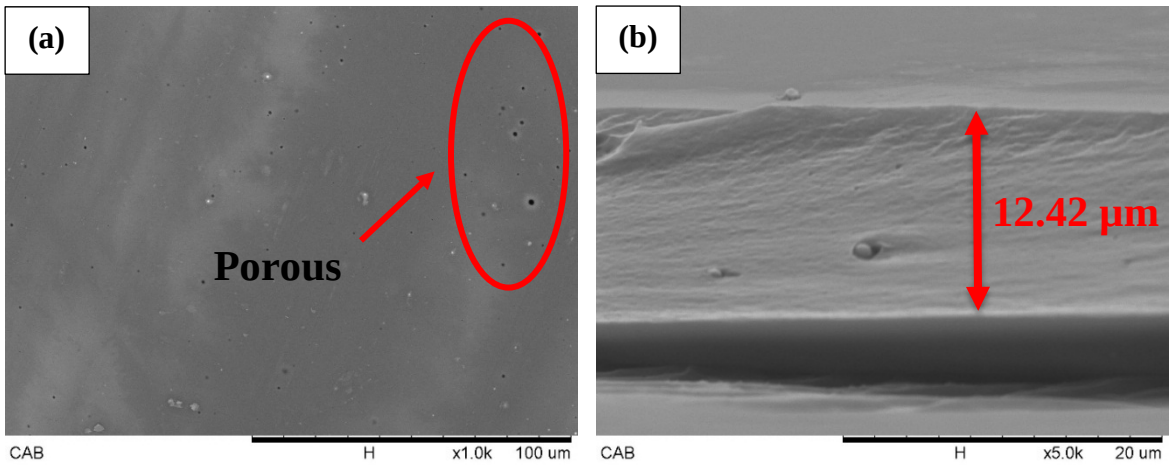

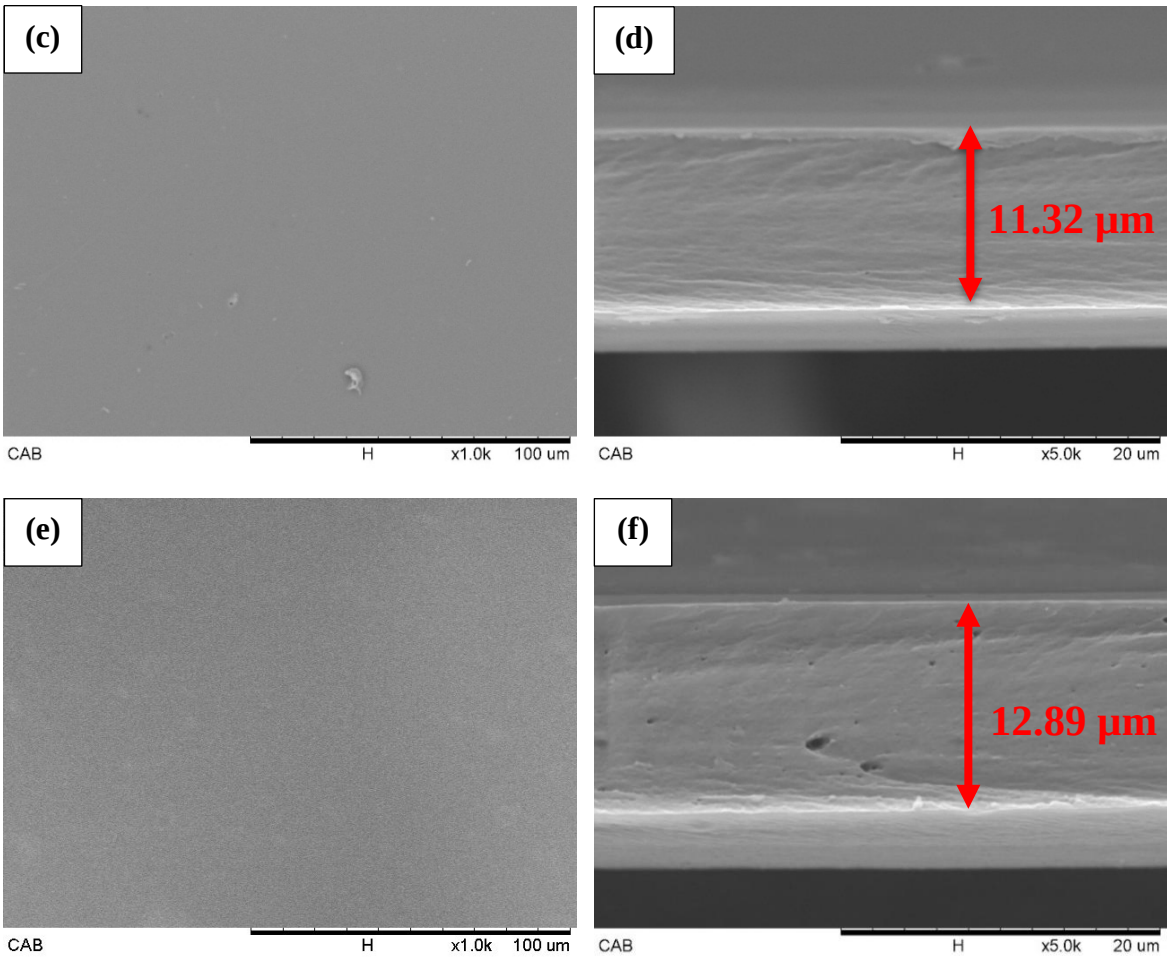

Fig 1. Top and cross-sectional SEM of CAB membrane at casting thickness (a-b) 200 µm (CAB-200), (c-d) 250 µm (CAB-250), and (e-f) 300 µm (CAB-300), with 4 wt% CAB polymer concentration and 5 minutes solvent evaporation time

The CO_2 permeance of CAB-200, CAB-250, and CAB-300 are illustrated in **Fig. 2**. Notably, CAB-250 demonstrated a higher permeance result of 398.46 ± 1.43 GPU, as compared to CAB-200 (143.03 ± 0.62 GPU) and CAB-300 (12.93 ± 0.34 GPU). This was because of the reduction in its membrane thickness (11.32 µm, **Fig. 1d**) and its selective smooth surface structure, which allowed the solution diffusion mechanism to occur efficiently. Therefore, the CO_2 permeance of CAB-250 increased (Jawad et al., 2015a). Meanwhile, the CO_2 permeance of CAB-300 reduced to 12.93 ± 0.34 GPU, indicating that a higher casting thickness beyond 250 µm can exert extra resistance towards gas diffusion within the membrane, which in turn affects the efficiency of gas permeation due to the thick dense membrane synthesised (**Fig. 1f**).

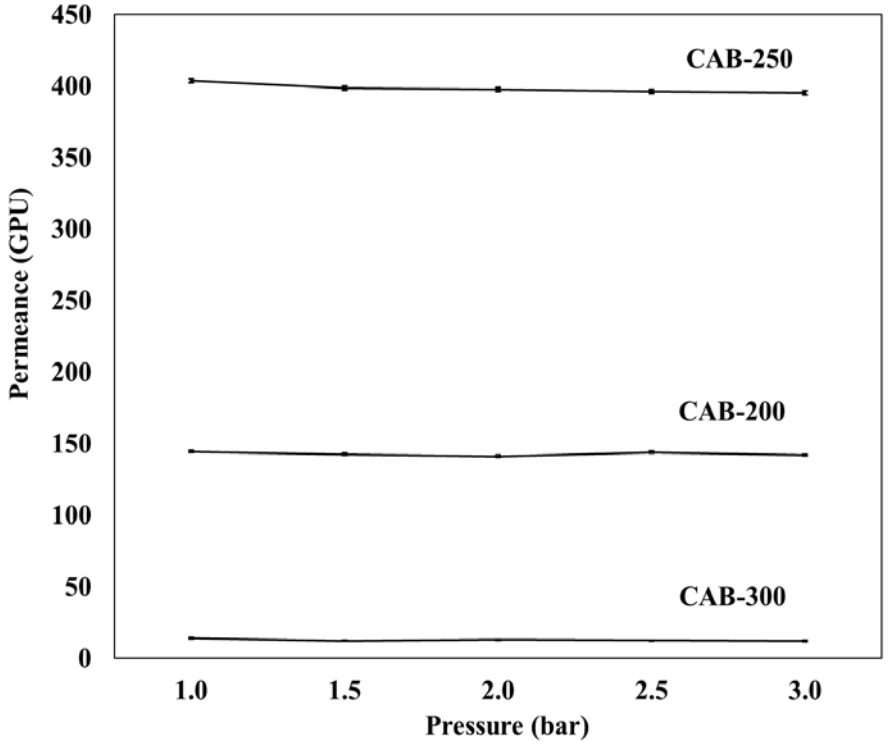

Fig 2. CO_2 permeance for membrane fabricated at 200 µm (CAB-200), 250 µm (CAB-250), and 300 µm (CAB-300), with 4 wt% CAB polymer concentration and 5 minutes solvent evaporation time

On the other hand, the N_2 permeance for CAB-200, CAB-250 and CAB-300 were 112.83 ± 0.85, 121.55 ± 1.30, and 11.26 ± 0.31 GPU, respectively, as illustrated in **Fig. 3**. The CAB-250 exhibited higher N_2 permeance results. This was due to the initial casting thickness applied, resulting in a smooth membrane structure, which created less resistance towards the permeance of N_2 gas within the membrane (Freeman, 1999). The low N_2 permeance result yield for CAB-300 (11.26 ± 0.31 GPU) was due mainly to the thick dense membrane structure (12.89 ± 0.10 µm), which ultimately governed the solution diffusion rate of the membrane, as a thicker membrane usually induces more resistance to gas diffusion (Koros et al., 1988a).

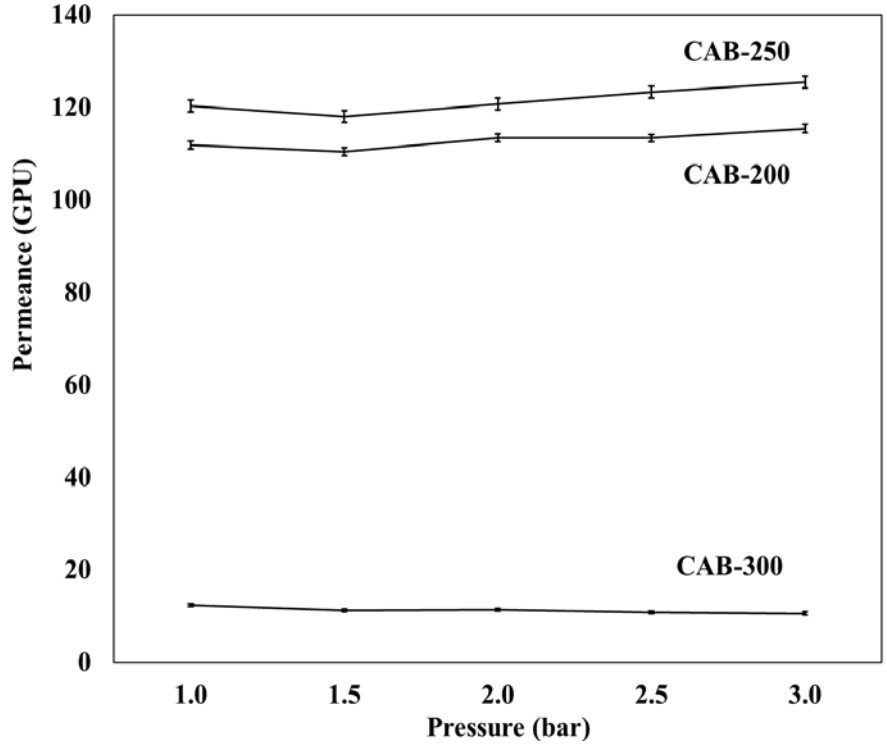

Fig 3. N_2 permeance for membrane fabricated at 200 µm (CAB-200), 250 µm (CAB-250), and 300 µm (CAB-300), with 4 wt% CAB polymer concentration and 5 minutes solvent evaporation time

The ideal selectivity of CO_2/N_2 separation performance for CAB-200, CAB-250, and CAB-300 are shown in **Fig. 4**. As observed from the results when increasing the casting thickness from 200 µm to 250 µm the selectivity increased from 1.27 ± 0.01 GPU (CAB-200) to 3.28 ± 0.04 GPU (CAB-250). The acceptable result obtained for CAB-250 was due to the membrane structure formation, which eventually increased the CO_2 permeance against the N_2 permeance attained. However, the selectivity reduced to 1.15 ± 0.01 GPU when the higher casting thickness (300 µm) was implemented for CAB-300. Even though the thickness of the membrane was essential for effective gas separation, however, excessive membrane thickness restricted the gas diffusion within the membrane.

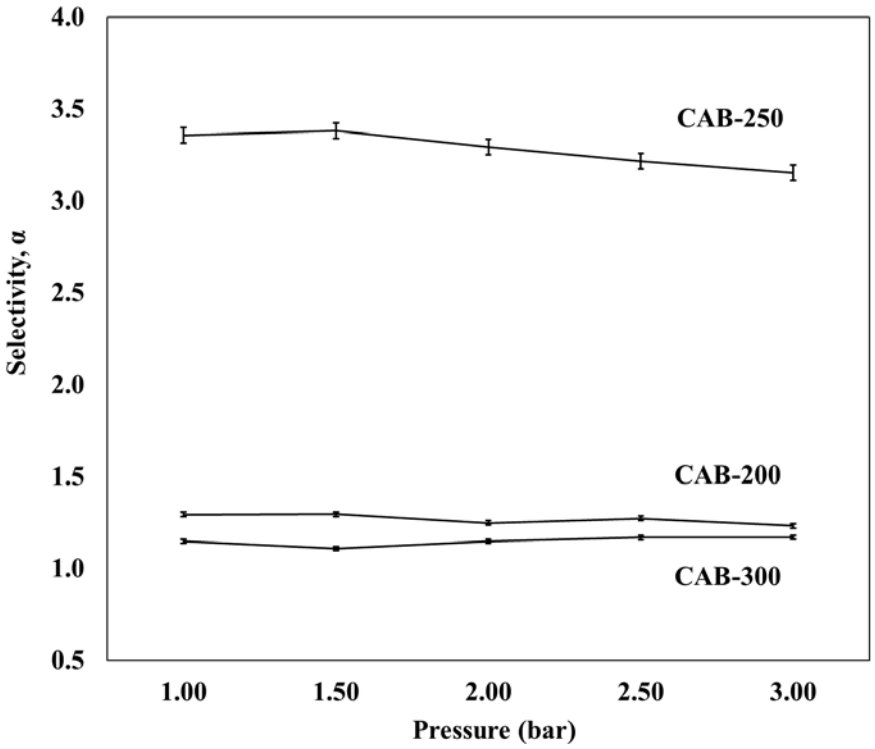

Fig 4. Ideal selectivity of CO_2/N_2 for membranes fabricated at different casting thickness 200 µm (CAB-200), 250 µm (CAB-250), and 300 µm (CAB-300), with 4 wt% CAB polymer concentration and 5 minutes solvent evaporation time

3.2 Effect of solvent exchange with Isopropyl alcohol

The solvent exchange was performed after the precipitation immersion process of the CAB membrane with the purpose of drying or removing any remaining volatile liquid in the membrane. As displayed in Figs**. 5a** and **b**, the CAB-15Iso (15 minutes) exhibited a porous surface and irregular dense cross-sectional structure with a membrane thickness of 13.87 ± 0.23 µm. This porous structure surface was caused by the rapid solvent exchange between the water molecules available within the CAB structure and the first solvent (isopropyl alcohol) (Lui et al., 1988). During the first step of the solvent exchange process, an enormous amount of water molecules embedded in the membrane were generally replaced by isopropyl alcohol. As a result, due to the short 15 minutes solvent exchange immersion period allocated, vigorous pore formation appeared throughout the film membrane of CAB-15Iso (Lui et al., 1988). Thus, CAB-15Iso demonstrated thick membrane thickness because of the short solvent exchange time applied, resulting in more water molecules retaining inside the membrane.

Meanwhile, when the isopropyl alcohol solvent exchange time was increased to 30 minutes (CAB-30Iso) and then subsequently to 60 minutes (CAB-60Iso), both revealed a smooth surface (**Figs. 5c** and **e**) with thin dense membrane thickness of 9.45 ± 0.06 µm and 9.30 ± 0.05 µm, respectively, as demonstrated in **Figs. 5d** and **f**. The formation of smooth surface and thin membrane was because of the longer immersion period allocated. Therefore, this provided more relaxation time for the non-solvent (H_2O) imbedded in the film membrane to exchange with the isopropyl alcohol (Radjabian et al., 2014). This also allowed the formation of a thin dense membrane with homogeneous smooth surface structure as revealed from CAB-30Iso and CAB-60Iso.

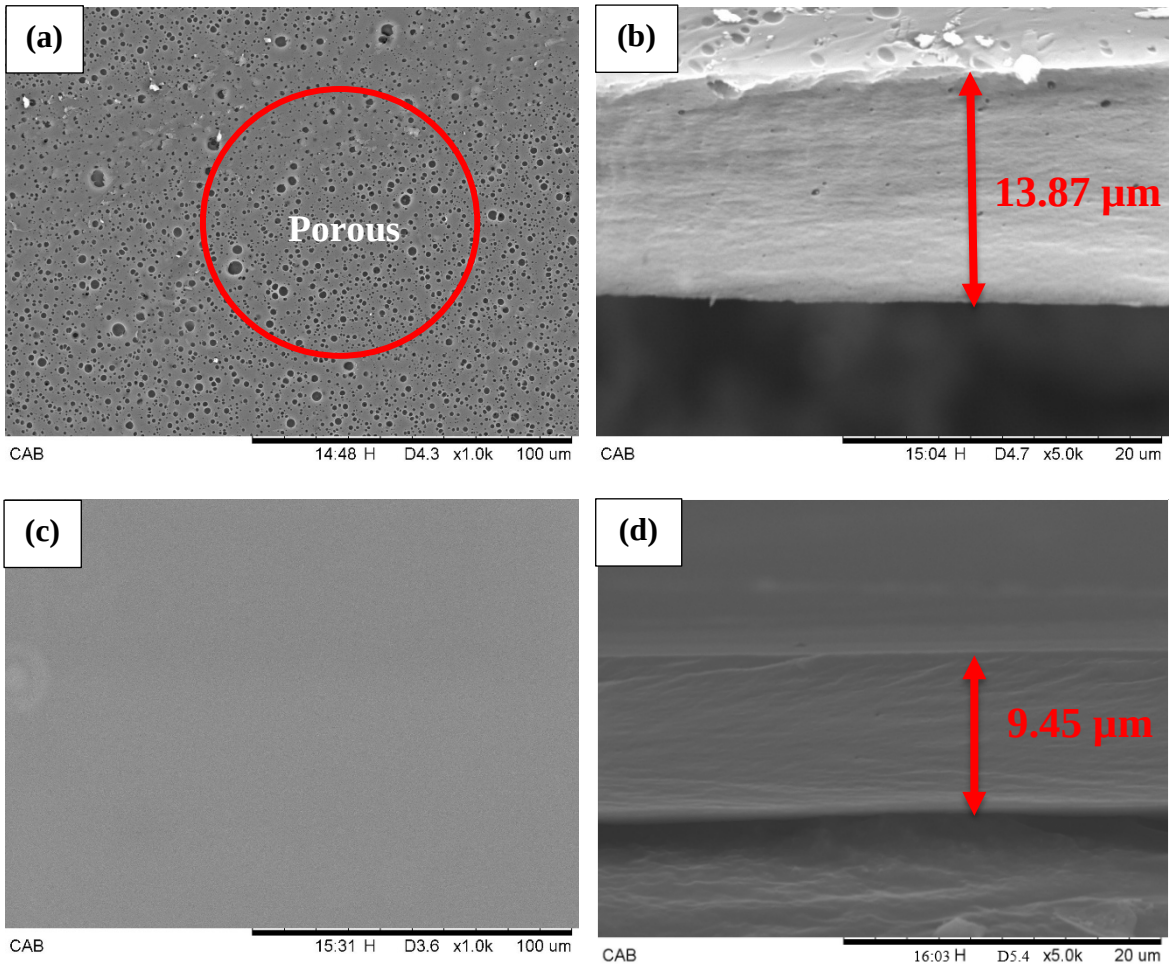

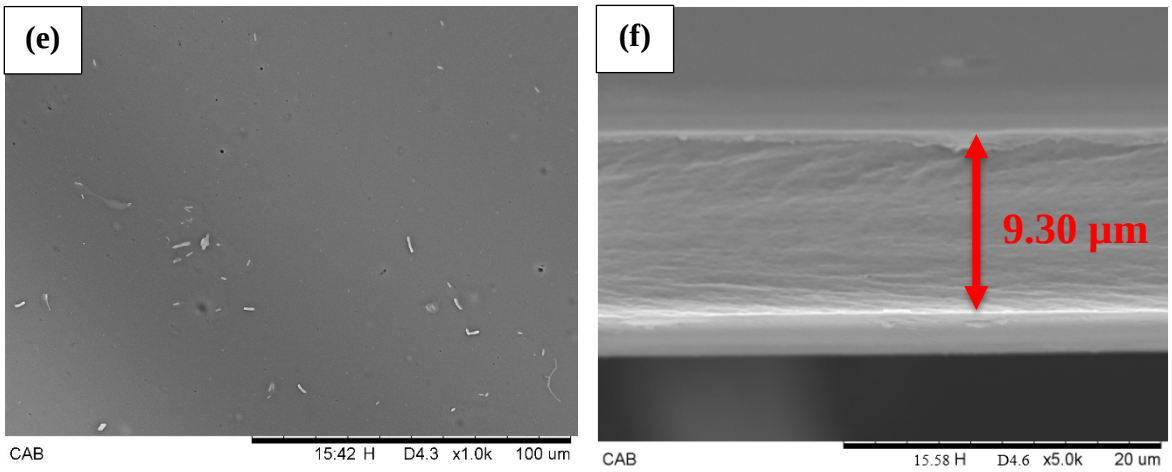

Fig 5. Surface and cross-sectional SEM of CAB membrane dried with isopropyl alcohol first for a solvent exchange duration of (a-b) 15 minutes (CAB-15Iso), (c-d) 30 minutes (CAB-30Iso), and (e-f) 60 minutes (CAB-60Iso); then subsequently solvent exchanged with 60 minutes of n-hexane as the final solvent, at casting thickness of 250 µm and 5 minutes solvent evaporation time

As shown in **Fig. 6**, the CO_2 permeance rates increased from 65.53 ± 0.34 GPU (CAB-15Iso) to 262.29 ± 0.16 GPU (CAB-30Iso) and increased further to 398.82 ± 0.94 GPU (CAB-60Iso) by changing the solvent exchange duration of isopropyl from 15 minutes to 30 minutes and subsequently to 60 minutes, respectively. This resulted in extensive water content reduction within the membrane structure due to longer immersion period allocated. The steady exchange rate of water with isopropyl alcohol within the CAB polymer matrix caused less CO_2 molecules to interact with the water, therefore allowing more CO_2 gas to permeate through the membrane (Jawad et al., 2015b). In the meantime, the high CO_2 permeance rate for CAB-60Iso (60 minutes) contributed to the thin dense membrane structure, which allowed the CO_2 feed gas to pass through the membrane with least resistance pathway as compared to the thick dense membrane (Tiraferri et al., 2011). Thus, the CAB-60Iso (60 minutes) yielded the highest CO_2 permeance rate amongst the other membranes (CAB-15Iso and CAB-30Iso).

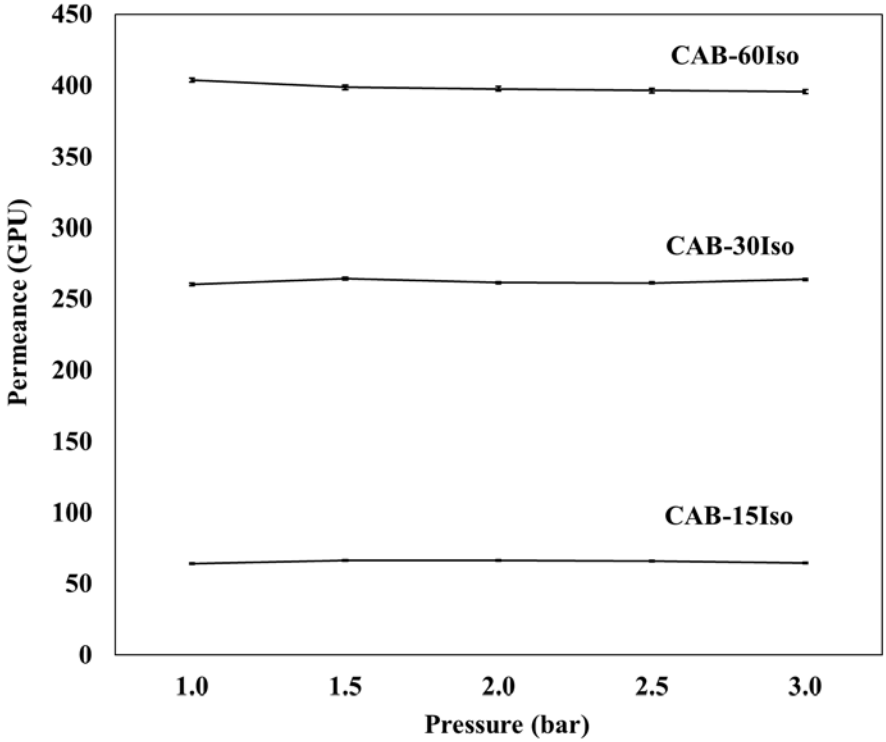

Fig 6. CO_2 permeance for membrane dried with 15 minutes (CAB-15Iso), 30 minutes (CAB-30Iso), and 60 minutes (CAB-60Iso) of isopropyl alcohol; then subsequently solvent exchanged with 60 minutes of n-hexane as the final solvent, at casting thickness of 250 µm and 5 minutes solvent evaporation time

The N_2 permeance rates for CAB-15Iso, CAB-30Iso, and CAB-60Iso are depicted in **Fig. 7**. The results obtained for N_2 permeance were 64.59 ± 0.41, 70.49 ± 0.33, and 121.76 ± 0.83 GPU for CAB-15Iso, CAB-30Iso, and CAB-60Iso, respectively. The possible explanation for this trend was due to the reduction in the membrane thickness from 13.87 µm to 9.3 µm (**Fig. 5**). In addition, as isopropyl alcohol was mainly made up from non-polar molecules, the remaining molecules within the CAB structure can easily attract light gas molecules (Katayama and Nitta, 1976). Thus, with longer solvent exchange duration, more isopropyl alcohol was retained within the polymer matrix, hence, attracting more N_2 gas molecules and resulting in the high N_2 permeance rate for CAB-60Iso (60 minutes). Eventually as the solvent exchange duration decreased, the N_2 permeance rate for CAB-15Iso and CAB-30Iso reduced as well.

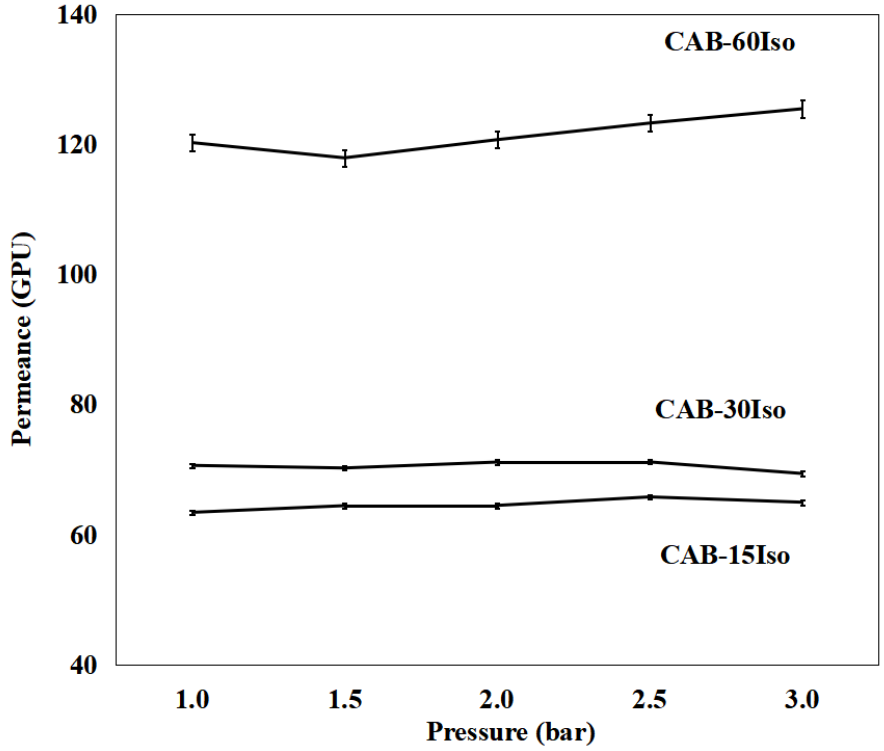

Fig 7. N_2 permeance for membrane dried with 15 minutes (CAB-15Iso), 30 minutes (CAB-30Iso), and 60 minutes (CAB-60Iso) of isopropyl alcohol; then subsequently solvent exchanged with 60 minutes of n-hexane as the final solvent, at casting thickness of 250 µm and 5 minutes solvent evaporation time

As discussed previously, CAB-60Iso (60 minutes) showed a thin dense membrane formation with high CO_2 and N_2 permeance rates. However, based on **Fig. 8,** the CAB-30Iso (30 minutes) yielded the best selectivity performance. This was due to the smooth homogeneous surface and superior cross-sectional morphology, which selectively allowed a predetermined amount of CO_2 and N_2 to pass through the dense membrane. On the contrary, the CAB-15Iso (15 minutes) demonstrated low selectivity (**Fig. 8)**. This was due to the presence of a thick irregular surface morphology (**Figs. 5a** and **b**), which imposed an undesirable effect on membrane permeance performance due to extra resistance pathway generated (Rahimpour et al., 2008, Yang and Wang, 2006). Therefore, CAB-30Iso (30 minutes) was preferred as compared to CAB-15Iso (15 minutes) and CAB-60Iso (60 minutes) because of its excellent morphology and good selectivity performance.

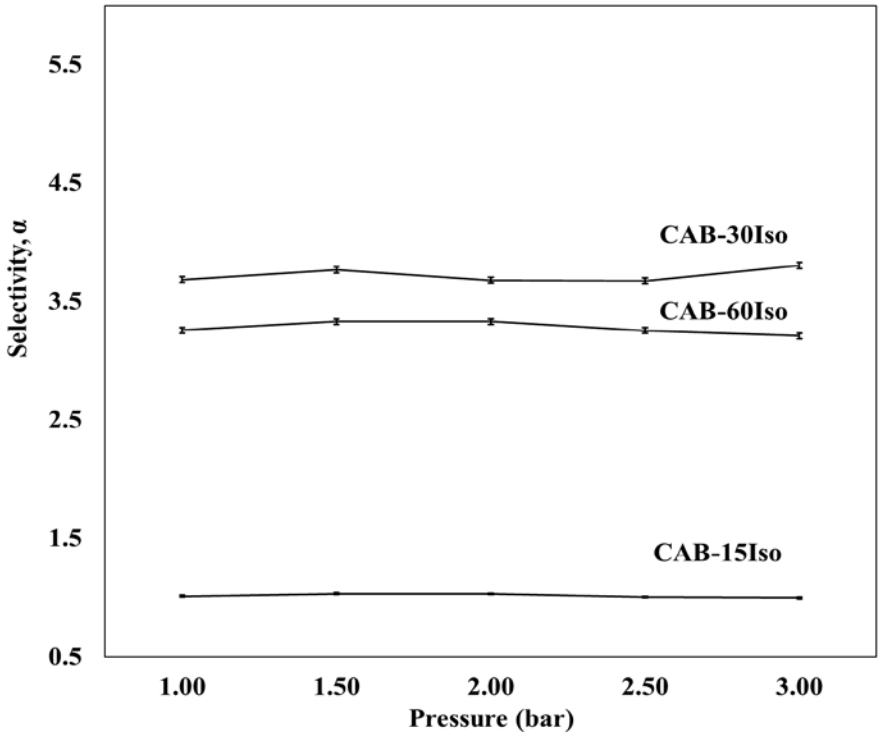

Fig 8. Ideal selectivity of CO_2/N_2 for membranes synthesised with solvent exchange duration of 15 minutes (CAB-15Iso), 30 minutes (CAB-30Iso), and 60 minutes (CAB-60Iso); then subsequently exchanged with 60 minutes of n-hexane as the final solvent, at casting thickness of 250 µm and 5 minutes solvent evaporation time

3.3 Effect of exchange time with n-hexane

As discussed in the previous section, the best solvent exchange time for isopropyl alcohol was 30 minutes (CAB-30Iso). Subsequently, the CAB membrane was subjected to further optimisation with the drying time of n-hexane. In this study, the CAB membranes were dried with solvent exchange times of 15 minutes (CAB-15H), 30 minutes (CAB-30H), and 60 minutes (CAB-60H) using n-hexane. As revealed from the SEM image in **Fig. 9**, the surface of CAB-15H (15 minutes) exhibited a porous structure, while CAB-30H (30 minutes) and CAB-60H (60 minutes) showed smooth surfaces. The main reason for the porous structure showed by CAB-15H was due to the rapid evaporation of the volatile solvent from the membrane structure itself and short duration of immersion period implemented (Chung and Kafchinski, 1997). Gradually by increasing the solvent exchange immersion period, the membrane had sufficient time for the solvent exchange to occur between isopropyl alcohol and n-hexane at a consistent and steady rate. Hence, suppressing a vigorous solvent exchange process within the polymer,

resulted in a smooth homogeneous surface as observed for CAB-30H (30 minutes) and CAB-60H (60 minutes) (Choi et al., 2006).

As presented in **Fig. 9**, the membrane thickness for CAB-15H (15 minutes), CAB-30H (30 minutes), and CAB-60H (60 minutes) were 11.79 ± 0.18, 9.50 ± 0.10, and 9.45 ± 0.06 µm, respectively. As seen from these results, the increased exchange time of n-hexane caused the CAB membrane to become more compact due to membrane densification as time passed (Sabde et al., 1997). In addition, the main reason for the reduction in the membrane thickness was due to the isopropyl alcohol imbedded within the membrane slowly being replaced by n-hexane with time. The replacement of isopropyl alcohol with n-hexane occurred when the molecular affinity of n-hexane was greater than isopropyl alcohol (Hansen, 2007). Referring to the Hansen solubility chart, the solubility for isopropyl alcohol, n-hexane, and water are 23.6, 14.9, and 47.9 $MPa^{1/2}$, respectively (Egan and Dufresne, 2008, Hansen, 2007). Therefore, the molecular affinity is in the order of CAB-water>CAB-isopropyl alcohol>CAB-n-hexane. The order of the molecular affinity represents the attraction force between the polymer and the solvent and non-solvent used (Kim and Oh, 2001).

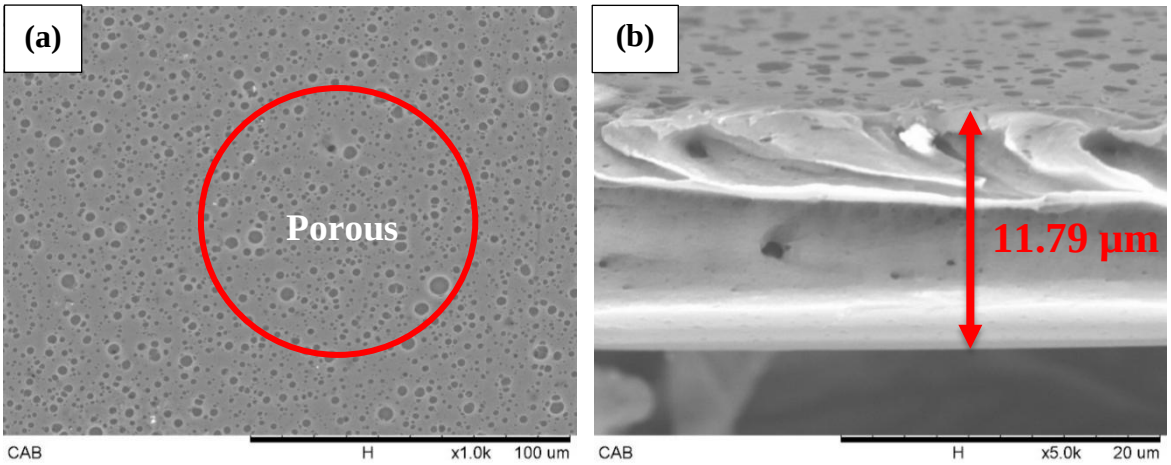

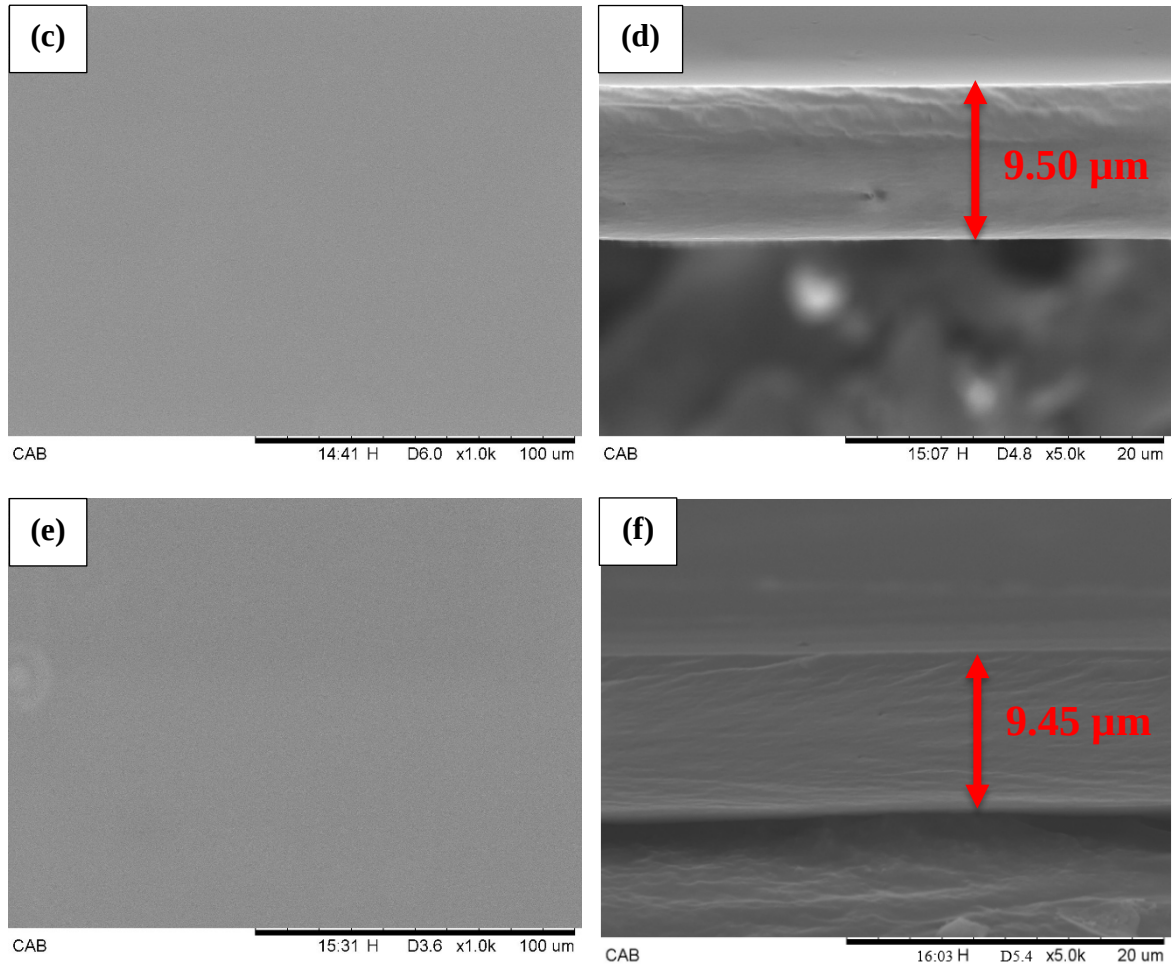

Fig 9. Surface and cross-sectional SEM of CAB membrane dried with 30 minutes of isopropyl alcohol first then followed by; (a-b) 15 minutes (CAB-15H), (c-d) 30 minutes (CAB-30H), and (e-f) 60 minutes (CAB-60H) of solvent exchange time using n-hexane, at casting thickness of 250 µm and 5 minutes solvent evaporation time

According to the CO_2 permeance results displayed in **Fig. 10**, there was clear indication that CAB-60H showed the highest CO_2 permeance rate followed by CAB-30H and subsequently, by CAB-15H. As seen in **Fig. 10**, the CO_2 permeance increased significantly from 21.55 ± 0.03 GPU to 227.95 ± 0.39 GPU when the solvent exchange time increased from 15 minutes (CAB-15H) to 30 minutes (CAB-30H). This was because when the exchange time was increased, sufficient time was provided for the exchange of the isopropyl alcohol content with n-hexane and therefore, generating a relatively thinner and compact cross-sectional membrane, which favoured CO_2 permeation through the membrane (Jawad et al., 2015b). In addition, the CO_2 permeance increased further when the solvent exchange duration was increased from 30 minutes to 60 minutes, as observed from CAB-30H (227.95

± 0.39 GPU) to CAB-60H (262.29 ± 0.16 GPU). The increase in the CO_2 permeance could be related to the increase in the number of the remaining polar n-hexane molecules within the membrane structure, resulting in a more active interaction with the CO_2 molecules and hence, higher CO_2 permeance yield (Jawad et al., 2015b).

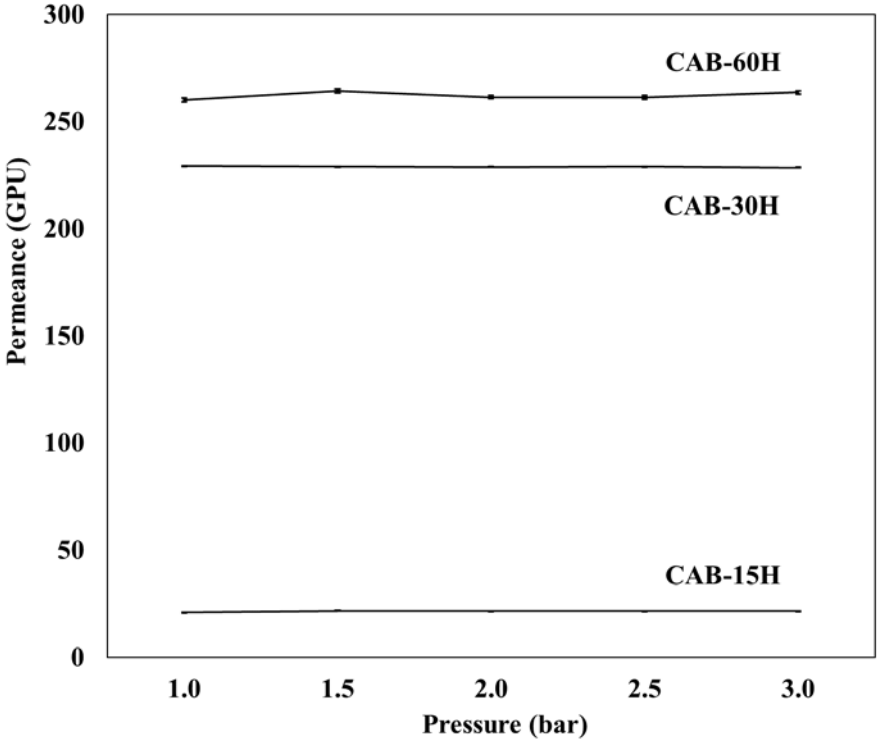

Fig 10. CO_2 permeance for membrane dried with 15 minutes (CAB-15H), 30 minutes (CAB-30H), and 60 minutes (CAB-60H) of n-hexane, at casting thickness of 250 µm and 5 minutes solvent evaporation time

Meanwhile, **Fig. 11** illustrated a drastic increase of N_2 permeance from 10.03 ± 0.02 GPU to 37.28 ± 0.54 GPU when the solvent exchange time of n-hexane was increased from 15 minutes (CAB-15H) to 30 minutes (CAB-30H). The reason for this increment was mainly due to the thin dense membrane structure of CAB-30H (9.50 ± 0.10 µm), which allowed the feed of N_2 gas to pass through a least resistance pathway. However, the high N_2 permeance for CAB-60H (70.49 ± 0.33 GPU) was due to stress of surface tension caused by high capillary forces because of the evaporation of residual n-hexane within the membrane, which led to the collapse in the structure (Matsuyama et al., 2002).

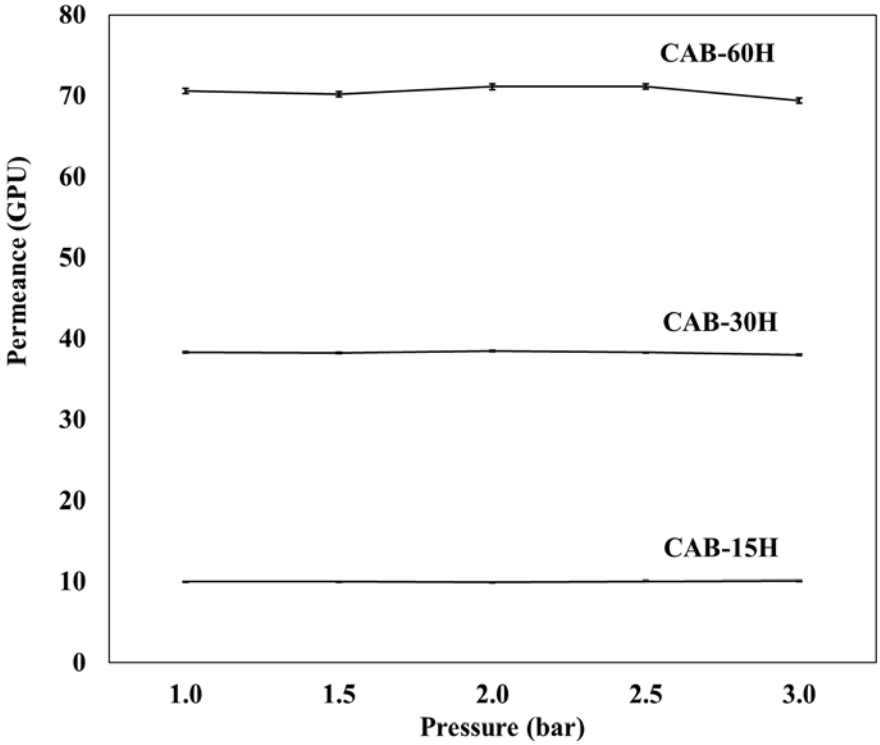

Fig 11. N_2 permeance for membrane dried with 15 minutes (CAB-15H), 30 minutes (CAB-30H), and 60 minutes (CAB-60H) of n-hexane, at casting thickness of 250 µm and 5 minutes solvent evaporation time

As seen in **Fig. 12**, the CAB-30H membrane showed the highest gas selectivity, which was achieved at 6.12 ± 0.09. This result further proved that to have a high gas separation performance a smooth surface with regular thin dense membrane morphology was preferable (**Figs. 9c** and **d**) (Huang and Feng, 1995, Jansen et al., 2005, Matsuyama et al., 2002, Lui et al., 1988). On the other hand, CAB-15H showed a lower separation performance of 2.15 ± 0.17. This was due to the collapse in the membrane structure caused by the short solvent immersion time, thereby generating an uneven porous surface and thick dense membrane structure, as presented in **Figs. 9a** and **b**. However, CAB-60H exhibited a smooth surface and thinner dense membrane morphology (9.45 ± 0.06 µm), as depicted in **Figs. 9e** and **f**. In addition, the low selectivity performance for CAB-60H (3.72 ± 0.03) was as a result of the excessive exchange time with n-hexane, which deformed the functionality of the membrane and therefore, generated moderate selectivity performance (Budd et al., 2005).

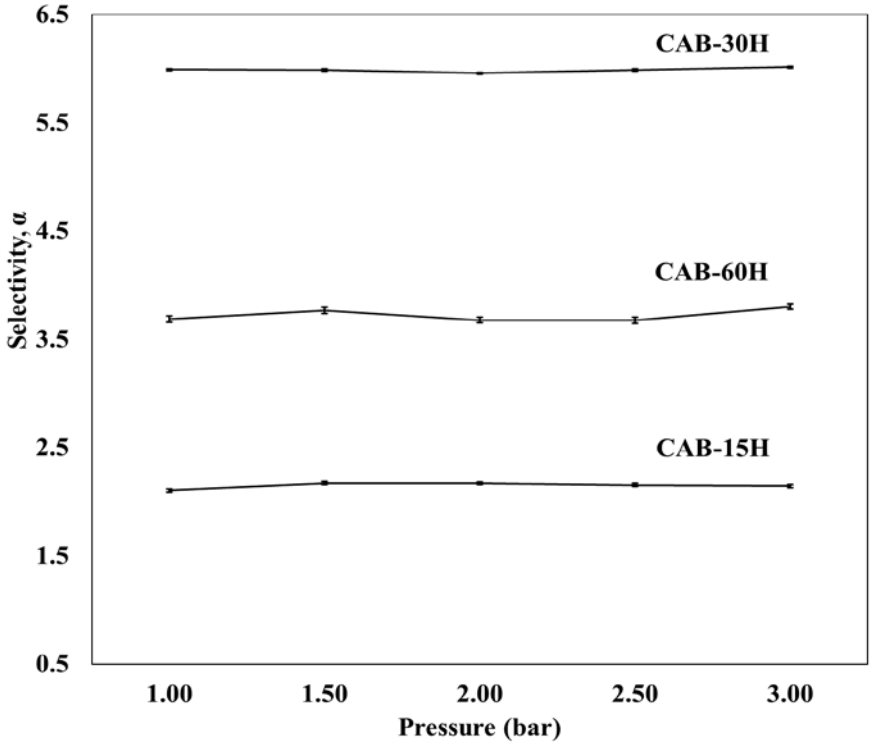

Fig 12. Ideal selectivity of CO_2/N_2 for CAB membrane dried with 30 minutes of isopropyl alcohol first then followed by; 15 minutes (CAB-15H), 30 minutes (CAB-30H), and 60 minutes (CAB-60H) of solvent exchange with n-hexane, at casting thickness of 250 µm and 5 minutes solvent evaporation time

3.4 The Effect of CAB polymer at different molecular weight (M_n)

According to Coltelli et al. (2008), the acetyl group has been deduced to have prominent effect on the membrane gas separation performance, as excessive acetyl composition in the membrane could promote plasticisation within the membrane (Coltelli et al., 2008, Ismail and Lorna, 2002). Thus, different CAB molecular weights with different acetyl, butyryl, and hydroxyl groups were investigated, as demonstrated in **Fig. 13**.

As depicted in **Figs. 13a** and **c**, a porous structure was observed for both CAB-12000 (M_n=12000) and CAB-65000 (M_n=65000), while CAB-70000 (M_n=70000) showed a smooth surface (**Fig. 13e**). The reason the membrane surface changed from porous to smooth was due to the high molecular weights of CAB, which caused the increase in the number of entanglements between the macromolecular chains in the solution (Jansen et al., 2006). Therefore, the high molecular weights of CAB favoured the gelation of the polymer rich phase after the phase-inversion occurred and hence, suppressed the formation of the porous structure during the early stages (Jansen et al., 2005).

Based on **Figs. 13b**, **d**, and **f**, the thickness of CAB-12000, CAB-65000, and CAB-70000 were 10.96 ± 0.10, 16.05 ± 0.17, and 9.50 ± 0.10 µm, respectively. The increment in the CAB molecular weights further influenced the membrane thickness through the rheological properties of the casting solution (Jansen et al., 2005). This was due to the high molecular weights of the CAB polymer being utilised for membrane fabrication, which gave the rapid gelation (Jansen et al., 2005). After the rapid gelation, the porous structure was greatly suppressed and further evaporation of solvent and non-solvent from the polymer matrix resulted in gradual shrinkage of the structure (Jansen et al., 2005). Therefore, the thickness of CAB-70000 (9.50 ± 0.10 µm) was thinner than CAB-12000 (10.96 ± 0.10 µm) and CAB-65000 (16.05 ± 0.17 µm).

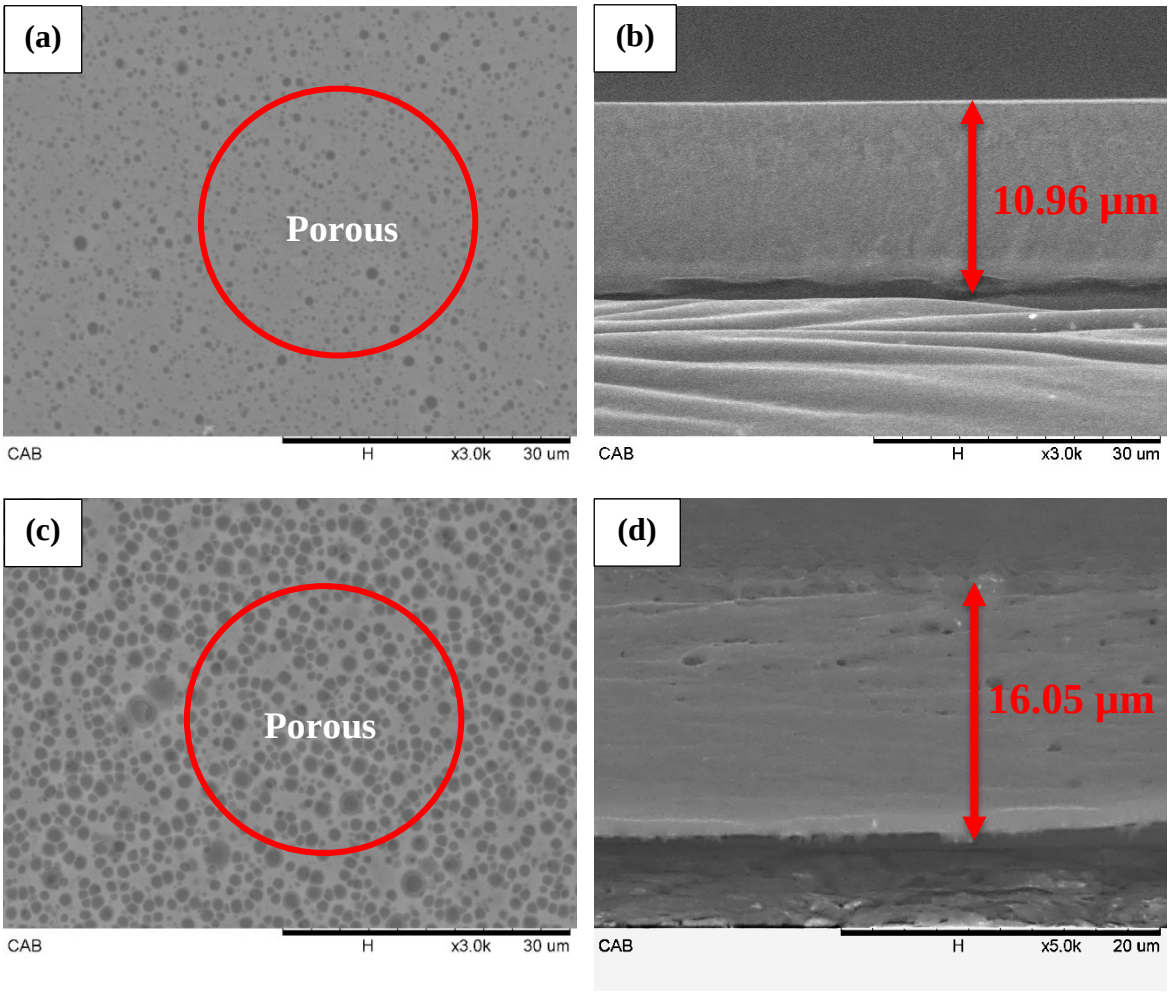

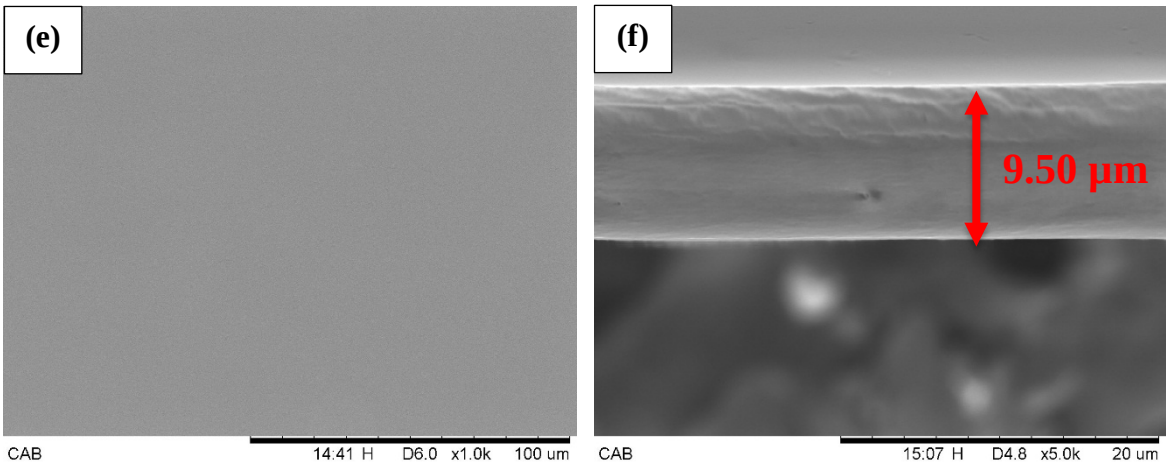

Fig 13. Surface and cross-sectional SEM of CAB membranes prepared with polymer concentration of 4 wt% and molecular weights (M_n) of (a-b) 12000 (CAB-12000), (c-d) 65000 (CAB-65000), and (e-f) 70000 (CAB-70000), at casting thickness of 250 µm and 5 minutes solvent evaporation time

The performance of CO_2 permeance achieved for the different molecular weights (M_n) of CAB-12000, CAB-65000, and CAB-70000 were 101.42 ± 0.97, 74.37 ± 1.25, and 227.95 ± 0.39 GPU, respectively, as shown in **Fig. 14**. The decrease in the CO_2 permeance rates observed from CAB-12000 (28-31 wt%) to CAB-65000 (16-19 wt%) was due to the thick dense membrane morphology as presented in **Fig. 13d** (16.05 ± 0.17 µm), which can hindrance the CO_2 permeance (Jawad et al., 2015a). Meanwhile, CAB-12000, which exhibited greater membrane thickness of 10.96 ± 0.10 µm, contradicted the results with higher CO_2 permeance, as illustrated in **Fig. 14**. The possible explanation for the increase in CO_2 permeance was caused by the acetyl groups rigidity and steric effects (Wan et al., 2003). Therefore, this allowed the higher intrinsic solubility of CO_2 due to the greater number of acetyl–acetyl interactions that existed (Koros et al., 1988b, Scholes et al., 2012). In addition, increasing the CAB molecular weight from 65000 to 70000 had increased the permeance rate drastically from 74.37 ± 1.25 GPU to 227.95 ± 0.39 GPU. Even though, CAB-70000 (12-15 wt%) has the lowest acetyl-acetyl interactions due to low acetyl group composition compared to other CAB polymers. The significant increase in the CO_2 permeance was due to the thin dense membrane exhibited for CAB-70000, as thin dense membrane usually impose less flux resistance for the membrane (Pandey and Chauhan, 2001). Therefore, the permeance of CO_2 was highest among all as the membrane thickness was the thinnest.

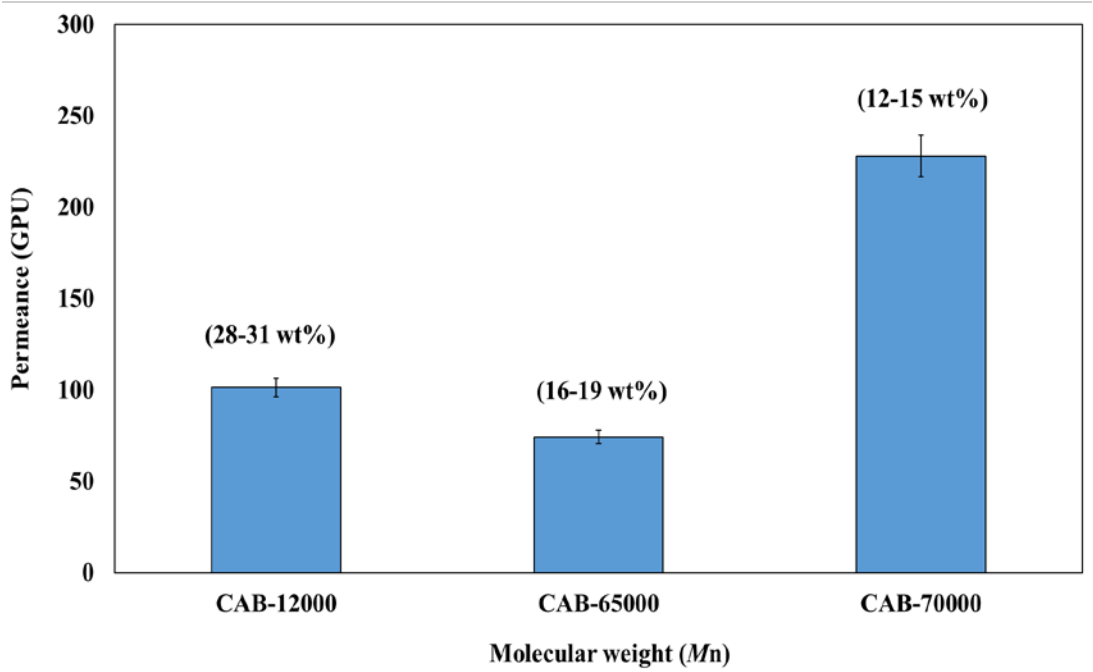

Fig 14. CO_2 permeance results for CAB membranes fabricated at different molecular weights comprising CAB-12000, CAB-65000, and CAB-70000 acetyl content of 28-31 wt%, 16-19 wt%, and 12-15wt%, respectively

As portrayed in **Fig. 15**, the N_2 permeance rate achieved for CAB-12000, CAB-65000, and CAB-70000 were 95.26 ± 1.06, 48.94 ± 0.89, and 37.28 ± 0.54 GPU, respectively. The reduction in N_2 permeance was due to the high presence of the hydroxyl group (1.2-2.2 wt%) content within the CAB-70000 polymer. The reaction between the hydroxyl and carbonyl groups of the CAB polymer caused the formation of hydrogen bonds, which could delay the de-mixing between the coagulant and the non-solvent. This resulted in the smooth homogeneous formation of the membrane surface, which could influence the N_2 permeance rate (Childress and Elimelech, 1996). Thus, it may be deduced that with the increment of the hydroxyl group within the membrane composition, the formation of a homogeneous surface morphology was favoured. Further, the hydroxyl group can increase the preferential restrictions on membrane pore formation, whereby the permeance and diffusion coefficient can be suppressed, hence, enhancing the selectivity performance of the membrane (Yave et al., 2009).

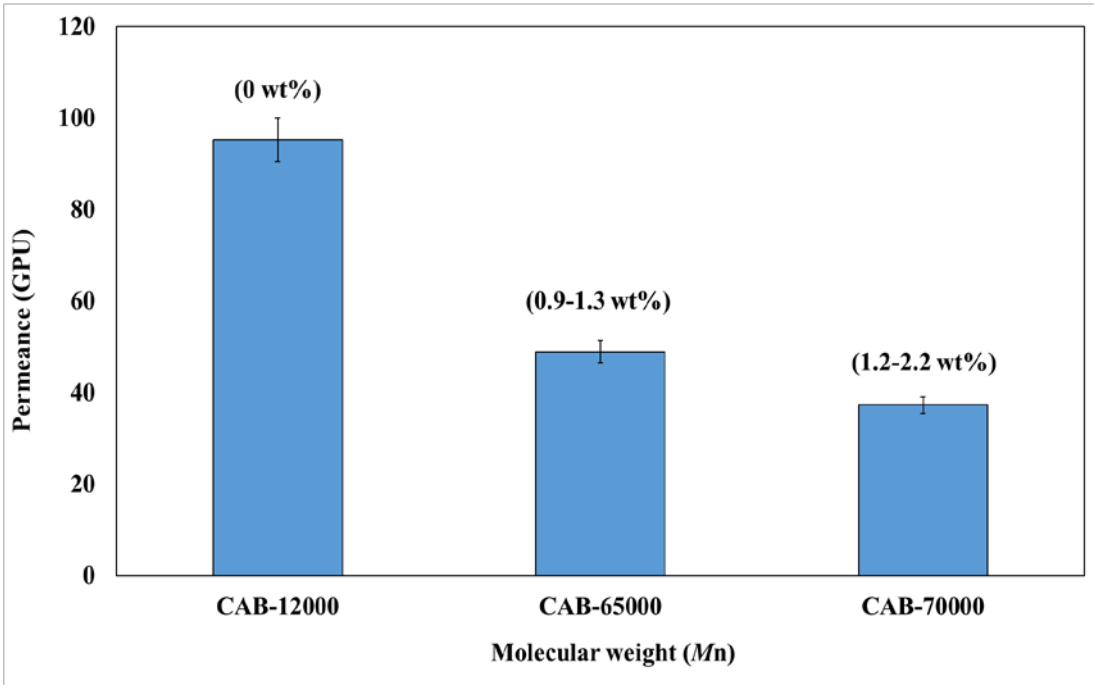

Fig 15. N_2 permeance results for CAB membranes synthesised at different molecular weights comprising CAB-12000, CAB-65000, and CAB-70000 hydroxyl content of 0 wt%, 0.9-1.3 wt%, and 1.2-2.2 wt%, respectively

Fig. 16 reveals the selectivity results for the different CAB molecular weights of 12000 (CAB-12000), 65000 (CAB-65000), and 70000 (CAB-70000), respectively. From the selectivity results depicted in **Fig. 16**, CAB-70000 achieved the average highest selectivity of 6.12 ± 0.09, followed by CAB-65000 with a moderate selectivity of 1.52 ± 0.04, and CAB-12000 with the lowest selectivity of 1.06 ± 0.01. The high selectivity performance of CAB-70000 was due to the high presence of the butyryl group content (35-39 wt%), which promoted the CO_2 diffusion better due to the increase of the non-polar butyryl chain within the structure of the membrane, thus, making the membrane more hydrophobic in nature (Wan et al., 2004, Ong et al., 2012).

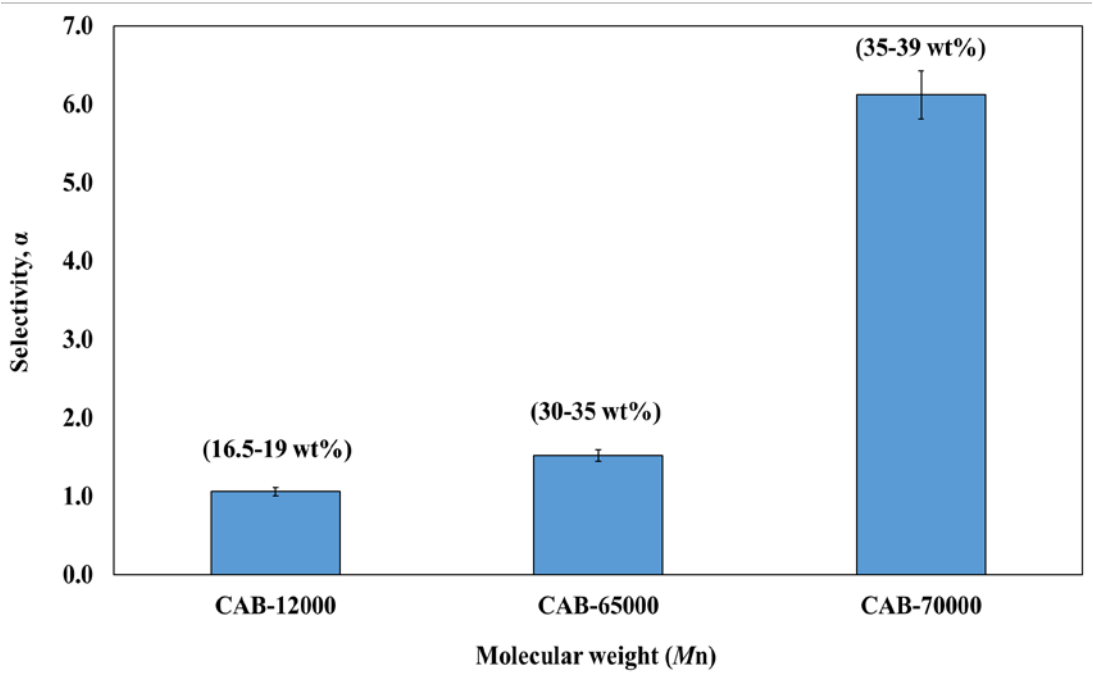

Fig 16. CO_2/N_2 selectivity results for CAB membranes at different molecular weights comprising CAB-12000, CAB-65000, and CAB-70000 butyryl content of 16.5-19 wt%, 30-35 wt%, and 35-39 wt%, respectively

362

363 *3.4.1 X-ray Photoelectron Spectroscopy (XPS) Analysis*

364 The XPS characterisation was adopted in this study to analyse the quantitative element composition of
365 the CAB membrane fabricated. The quantitative element composition of the membrane surface can be
366 determined from the spectrum obtained. Consequently, CAB-12000, CAB-65000, and CAB-70000 were
367 analysed through XPS analysis. The surface chemical quantitative compositions are depicted in **Table**
368 **1** and **Fig. 17**, respectively.

369 Observing the results tabulated in **Table 1**, both the atomic and mass concentration of the oxygen
370 (O) atom decreased with the increase in the CAB membrane molecular weights. The decreasing trend
371 of atomic concentration from 34.02>30.88>27.30% and mass concentration from 40.72>37.31>33.35%
372 of the O atom was due to the decrease of the acetyl group derived from each CAB polymer
373 (Suttiwijitpukdee et al., 2011). As indicated clearly in **Fig. 14**, the acetyl group affected the permeance
374 of CO_2 within the membrane. Hence, this further proved that increasing the acetyl group or O atom
375 presence within the membrane subsequently, decreased the permeance of CO_2. The increase in the O
376 element was mainly funded by the breaking of the carbonyl (C=O) group and prompted the formation

of a new carboxyl group (-COOH) (Liu et al., 2014). The increase in carboxyl group made the membrane more hydrophilic, resulting in decline of the CO_2 permeance flux (Xia and Ni, 2015, Xu et al., 2014).

Table 1. Element composition of the CAB membrane synthesized at different molecular weight

Peak	CAB-12000		CAB-65000		CAB-70000	
	Atomic Conc %	Mass Conc %	Atomic Conc %	Mass Conc %	Atomic Conc %	Mass Conc %
O 1s	34.02	40.72	30.88	37.31	27.30	33.35
C 1s	65.98	59.28	69.12	62.69	72.70	66.65

On the other hand, when observing the carbon (C) element present within CAB-12000, CAB-65000, and CAB-70000, the C atoms increased with increase in the polymer molecular weights. The atomic concentration increased from 65.98>69.12>72.70 and the mass concentration increased from 59.28>62.69>66.65 for CAB-12000, CAB-65000, and CAB-70000, respectively. The increase in the C element within the membrane was because of the increase in the butyryl group within the CAB polymer. As indicated in **Fig. 16**, the butyryl group played a crucial role in manipulating the selectivity performance of the membrane, because it can increase the CO_2 diffusion due to the increase of the non-polar butyryl chain within the structure of the membrane (Wan et al., 2004). As a result the membrane became more hydrophobic in nature, and hence, promoted better CO_2 permeance flux (Ong et al., 2012).

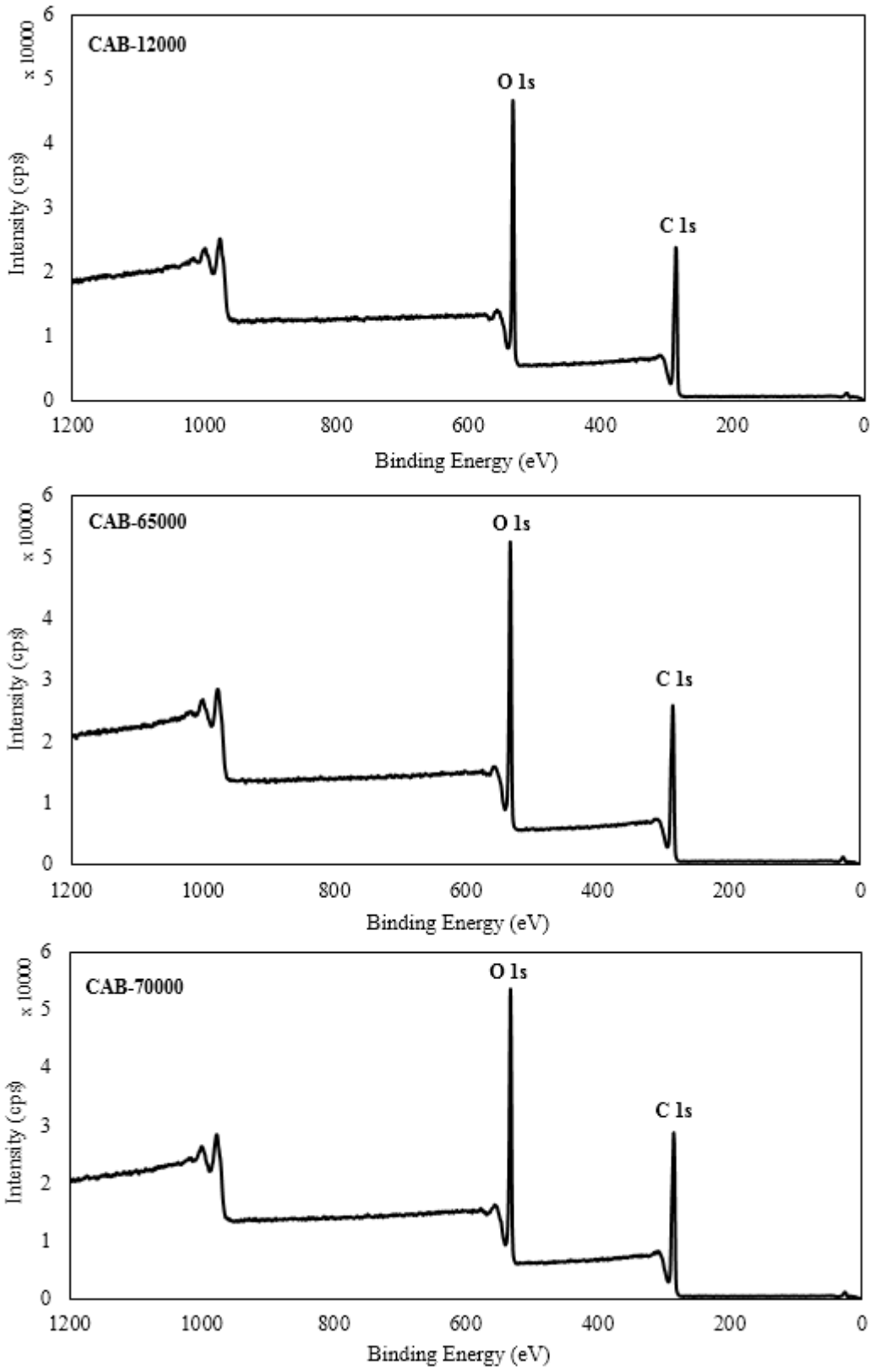

Fig 17. Element composition of XPS spectrum of CAB-12000, CAB-65000, and CAB-70000

The CO_2/N_2 separation performance of this current study were summarised and compared with other research works, as shown in **Table 2**. In this study, the best membrane performance achieved for both CO_2 permeance and selectivity was 227.95 ± 0.39 GPU and 6.12 ± 0.09, respectively for CAB-70000. This was a result of the dynamic contents of acetyl, butyryl, and hydroxyl composition present in CAB polymer. The acetyl and butyryl contributed significantly towards the permeance of CO_2/N_2 by enhancing the solubility of CO_2 within the membrane structure. As compared to other research works, the permeance results achieved in the present work showed higher CO_2/N_2 permeance with acceptable selectivity result. The selectivity performance achieved for this study shows the typical trade-off relationship of polymer membrane due to the high permeance results and low selectivity of the CAB polymer. Nevertheless, the low selectivity of the CAB polymer can eventually be overcome by incorporating the polymer matrix with inorganic filler to produce the hybrid system of mixed matrix membranes (MMMs) (Aroon et al., 2013, Chung et al., 2007, Ismail et al., 2009, Goh et al., 2011).

Table 2. List of CO_2/N_2 permeation results achieved from current study with previous work

Polymer	P (CO_2)	P (N_2)		Conditions	References
CAB	164.84 ± 0.73[a]	26.36 ± 0.05[a]	6.06 ± 0.23	1-3 x10^5 Pa, casting thickness of 250µm	Present work
SPEEK	5.01	1.94	5.58	1-1.5x10^5 Pa, 25 ºC, casting thickness of 60-80µm	(Xin et al., 2015)
BPPO	76.78 [b]	N/A	30	0.7x10^5 Pa, casting thickness of 50-90 µm	(Cong et al., 2007)
PES	10.98 [a]	0.80 [a]	13.73	3-4x10^5 Pa, casting thickness of 150µm	(Ismail et al., 2011)
6FDA-durene	30.3 [b]	2.87 [b]	10.56	35ºC, 10atm, casting thickness of 40µm	(Liu et al., 2001)

SPEEK- sulfonated polyetheretherketone, BPPO- brominated polyphenylene oxide, PES- polyethersulfone, 6FDA- 2,2-bis(3,4-dicarboxyphenyl) hexafluoropropane dianhydride

[a] GPU. [b] Barrer. N/A- not available.

4.0 Conclusion

The optimisation of membrane morphology conducted with respect to the different parameters was found to be successful for the preparation of the highly selective CAB gas separation membrane. The

membrane formation and morphology were closely related to the rheological behaviour of the casting solution. The results have shown that membrane casting thickness, solvent exchange duration for both isopropyl alcohol and n-hexane, and the molecular weights of the CAB polymer had a significant role in manipulating the CO_2/N_2 gas separation performance as well as the morphology of the membranes. Under optimised conditions, the best membrane was found to be the CAB-70000, which was fabricated with 4 wt% polymer concentration, 250 µm casting thickness, 5 minutes solvent evaporation time, 30 minutes solvent exchange with isopropyl alcohol followed by another 30 minutes of solvent exchange with n-hexane. Moreover, the CAB-70000 had the best gas separation performance with an average selectivity of 6.12 ± 0.09 and permeance up to 227.95 ± 0.39 GPU for CO_2 and 37.28 ± 0.54 GPU for N_2, respectively. The superior CO_2/N_2 separation performance of the membrane was mainly contributed by the quality formation of the smooth surface, with thin dense and defect-free membrane structure. Further, it has been suggested that to improve the performance of the CAB membrane, inorganic nanoparticle fillers such as carbon nanotubes (CNTs) be incorporated to produce mixed matrix membrane (MMM).

Acknowledgement

The authors would like to extend their appreciation to the Ministry of Higher Education Malaysia (MOHE) for providing Fundamental Research Grant Scheme (FRGS) (MOHE Ref. No: FRGS/1/2015/TK02/CURTIN/03/1) and Cost Centre: 001048. Further, the authors would also like to thank LRGS USM (Account No: 304/PJKIMIA/6050296/U124), and Curtin Cost Centre: 001047.

Keywords: Membrane gas separation; Cellulose acetate butyrate; casting thickness; solvent exchange time; isopropyl alcohol; n-hexane; molecular weight; functional groups; Scanning Electron Micrograph; X- ray Photoelectron Spectroscopy

References

Ahmad, A., Ideris, N., Ooi, B., Low, S. and Ismail, A. 2013. Synthesis of polyvinylidene fluoride (PVDF) membranes for protein binding: Effect of casting thickness. *Journal of Applied Polymer Science,* 128**,** 3438-3445.

Ahmad, A., Jawad, Z., Low, S. and Zein, S. 2014. A cellulose acetate/multi-walled carbon nanotube mixed matrix membrane for CO_2/N_2 separation. *Journal of Membrane Science,* 451**,** 55-66.

Aroon, M. A., Ismail, A. F. and Matsuura, T. 2013. Beta-cyclodextrin functionalized MWCNT: A potential nano-membrane material for mixed matrix gas separation membranes development. *Separation and Purification Technology,* 115**,** 39-50.

Barnes, R. J., Bandi, R. R., Chua, F., Low, J. H., Aung, T., Barraud, N., Fane, A. G., Kjelleberg, S. and Rice, S. A. 2014. The roles of Pseudomonas aeruginosa extracellular polysaccharides in biofouling of reverse osmosis membranes and nitric oxide induced dispersal. *Journal of Membrane Science,* 466**,** 161-172.

Basu, S., Khan, A. L., Cano-Odena, A., Liu, C. and Vankelecom, I. F. J. 2010. Membrane-based technologies for biogas separations. *Chemical Society Reviews,* 39**,** 750-768.

Budd, P. M., Msayib, K. J., Tattershall, C. E., Ghanem, B. S., Reynolds, K. J., Mckeown, N. B. and Fritsch, D. 2005. Gas separation membranes from polymers of intrinsic microporosity. *Journal of Membrane Science,* 251**,** 263-269.

Carapellucci, R. and Milazzo, A. 2003. Membrane systems for CO_2 capture and their integration with gas turbine plants. *Proceedings of the Institution of Mechanical Engineers, Part A: Journal of Power and Energy,* 217**,** 505-517.

Childress, A. E. and Elimelech, M. 1996. Effect of solution chemistry on the surface charge of polymeric reverse osmosis and nanofiltration membranes. *Journal of membrane science,* 119**,** 253-268.

Choi, J. H., Jegal, J. and Kim, W. N. 2006. Fabrication and characterization of multi-walled carbon nanotubes/polymer blend membranes. *Journal of Membrane Science,* 284**,** 406-415.

Chung, T. S., Jiang, L. Y., Li, Y. and Kulprathipanja, S. 2007. Mixed matrix membranes (MMMs) comprising organic polymers with dispersed inorganic fillers for gas separation. *Progress in Polymer Science,* 32**,** 483-507.

Chung, T. and Kafchinski, E. R. 1997. The effects of spinning conditions on asymmetric 6FDA/6FDAM polyimide hollow fibers for air separation. *Journal of applied polymer science,* 65**,** 1555-1569.

Coltelli, M. B., Maggiore, I. D., Bertoldo, M., Signori, F., Bronco, S. and Ciardelli, F. 2008. Poly (lactic acid) properties as a consequence of poly (butylene adipate-co-terephthalate) blending and acetyl tributyl citrate plasticization. *Journal of Applied Polymer Science,* 110, 1250-1262.

Cong, H., Zhang, J., Radosz, M. and Shen, Y. 2007. Carbon nanotube composite membranes of brominated poly (2, 6-diphenyl-1, 4-phenylene oxide) for gas separation. *Journal of Membrane Science,* 294**,** 178-185.

Conti, J., Holtberg, P., Diefenderfer, J., Larose, A., Turnure, J.T. and Westfall, L., 2016. *International Energy Outlook 2016 With Projections to 2040* (No. DOE/EIA--0484 (2016)). USDOE Energy Information Administration (EIA), Washington, DC (United States). Office of Energy Analysis.

Egan, W. M. and Dufresne, R. E. 2008. Gelled adhesive remover composition and method of use. U.S. Patent 7,977,294.

Feng, Y., Zhang, J. M., Zhang, J. and Chang, J. 2015. Gas Separation Properties of Cellulose Acetate Butyrate/MWCNTs Mixed Matrix Membranes. *ACTA POLYMERICA SINICA***,** 1396-1401.

Freeman, B. D. 1999. Basis of permeability/selectivity tradeoff relations in polymeric gas separation membranes. *Macromolecules,* 32**,** 375-380.

Goh, P. S., Ismail, A. F., Sanip, S. M., Ng, B. C. and Aziz, M. 2011. Recent advances of inorganic fillers in mixed matrix membrane for gas separation. *Separation and Purification Technology,* 81**,** 243-264.

Hansen, C. M. 2007. *Hansen solubility parameters: a user's handbook,* CRC press.

Huang, R. Y. and Feng, X. 1995. Studies on solvent evaporation and polymer precipitation pertinent to the formation of asymmetric polyetherimide membranes. *Journal of applied polymer science,* 57**,** 613-621.

Ismail, A. F., Goh, P. S., Sanip, S. M. and Aziz, M. 2009. Transport and separation properties of carbon nanotube-mixed matrix membrane. *Separation and Purification Technology,* 70**,** 12-26.

Ismail, A. F. and Lorna, W. 2002. Penetrant-induced plasticization phenomenon in glassy polymers for gas separation membrane. *Separation and purification technology,* 27**,** 173-194.

Ismail, A. F., Rahim, N., Mustafa, A., Matsuura, T., Ng, B. C., Abdullah, S. and Hashemifard, S. A. 2011. Gas separation performance of polyethersulfone/multi-walled carbon nanotubes mixed matrix membranes. *Separation and purification technology,* 80**,** 20-31.

Jansen, J. C., Buonomenna, M. G., Figoli, A. and Drioli, E. 2006. Asymmetric membranes of modified poly (ether ether ketone) with an ultra-thin skin for gas and vapour separations. *Journal of membrane science,* 272**,** 188-197.

Jansen, J. C., Macchione, M., Oliviero, C., Mendichi, R., Ranieri, G. A. and Drioli, E. 2005. Rheological evaluation of the influence of polymer concentration and molar mass distribution on the formation and performance of asymmetric gas separation membranes prepared by dry phase inversion. *Polymer,* 46**,** 11366-11379.

Jawad, Z., Ahmad, A., Low, S. and Zein, S. 2015a. Incorporation of inorganic carbon nanotubes fillers into the CA polymeric matrix for improvement in CO_2/N_2 separation. *Current Nanoscience,* 11**,** 69-79.

Jawad, Z. A., Ahmad, A. L., Low, S. C., Chew, T. L. and Zein, S. H. S. 2015b. Influence of solvent exchange time on mixed matrix membrane separation performance for CO_2/N_2 and a kinetic sorption study. *Journal of Membrane Science,* 476**,** 590-601.

Kappel, C., Kemperman, A., Temmink, H., Zwijnenburg, A., Rijnaarts, H. and Nijmeijer, K. 2014. Impacts of NF concentrate recirculation on membrane performance in an integrated MBR and NF membrane process for wastewater treatment. *Journal of membrane science,* 453**,** 359-368.

Katayama, T. and Nitta, T. 1976. Solubilities of hydrogen and nitrogen in alcohols and n-hexane. *Journal of Chemical and Engineering Data,* 21**,** 194-196.

Kim, C. S. and Oh, S. M. 2001. Performance of gel-type polymer electrolytes according to the affinity between polymer matrix and plasticizing solvent molecules. *Electrochimica acta,* 46**,** 1323-1331.

Koros, W., Fleming, G., Jordan, S., Kim, T. and Hoehn, H. 1988a. Polymeric membrane materials for solution-diffusion based permeation separations. *Progress in Polymer Science,* 13**,** 339-401.

Koros, W. J., Fleming, G. K., Jordan, S. M., Kim, T. H. and Hoehn, H. H. 1988b. Polymeric membrane materials for solution-diffusion based permeation separations. *Progress in Polymer Science,* 13**,** 339-401.

Kunthadong, P., Molloy, R., Worajittiphon, P., Leekarkpai, T., Kaabbuathong, N. and Punyodom, W. 2015. Biodegradable Plasticized Blends of Poly(L-lactide) and Cellulose Acetate Butyrate: From Blend Preparation to Biodegradability in Real Composting Conditions. *Journal of Polymers and the Environment,* 23**,** 107-113.

Lalia, B. S., Kochkodan, V., Hashaikeh, R. and Hilal, N. 2013. A review on membrane fabrication: Structure, properties and performance relationship. *Desalination,* 326**,** 77-95.

Lee, R., Jawad, Z., Ahmad, A., Ngo, J. and Chua, H. 2017. Improvement of CO_2/N_2 separation performance by polymer matrix cellulose acetate butyrate. In *IOP Conference Series: Materials Science and Engineering* (Vol. 206, No. 1, p. 012072). IOP Publishing.

Liu, L. F., Cai, Z. B., Shen, J. N., Wu, L. X., Hoek, E. M. and Gao, C. J. 2014. Fabrication and characterization of a novel poly (amide-urethane imide) TFC reverse osmosis membrane with chlorine-tolerant property. *Journal of Membrane Science,* 469**,** 397-409.

Liu, Y., Wang, R. and Chung, T. S. 2001. Chemical cross-linking modification of polyimide membranes for gas separation. *Journal of Membrane Science,* 189**,** 231-239.

Low, B. T., Zhao, L., Merkel, T. C., Weber, M. and Stolten, D. 2013. A parametric study of the impact of membrane materials and process operating conditions on carbon capture from humidified flue gas. *Journal of Membrane Science,* 431**,** 139-155.

Lui, A., Talbot, F., Fouda, A., Matsuura, T. and Sourirajan, S. 1988. Studies on the solvent exchange technique for making dry cellulose acetate membranes for the separation of gaseous mixtures. *Journal of applied polymer science,* 36**,** 1809-1820.

Matsuyama, H., Kim, M. M. and Lloyd, D. R. 2002. Effect of extraction and drying on the structure of microporous polyethylene membranes prepared via thermally induced phase separation. *Journal of Membrane Science,* 204**,** 413-419.

Ohya, H., Akimoto, N. and Negishi, Y. 1980. Reverse osmosis separation characteristics of organic solutes with cellulose acetate butyrate membranes. 5**,** 179-184.

Ong, R. C., Chung, T. S., Helmer, B. J. and De Wit, J. S. 2012. Novel cellulose esters for forward osmosis membranes. *Industrial and engineering chemistry research,* 51**,** 16135-16145.

Radjabian, M., Koll, J., Buhr, K., Vainio, U., Abetz, C., Handge, U. A. and Abetz, V. 2014. Tailoring the morphology of self-assembled block copolymer hollow fiber membranes. *Polymer,* 55**,** 2986-2997.

Rahimpour, A., Madaeni, S., Taheri, A. and Mansourpanah, Y. 2008. Coupling TiO_2 nanoparticles with UV irradiation for modification of polyethersulfone ultrafiltration membranes. *Journal of Membrane Science,* 313**,** 158-169.

Pandey, P. and Chauhan, R.S., 2001. Membranes for gas separation. *Progress in Polymer Science*, *26*(6), pp.853-893.

Paradise, M. and Goswami, T. 2007. Carbon nanotubes – Production and industrial applications. *Materials and Design,* 28**,** 1477-1489.

S.Minhas, B. 1992. Cellulose Acetate Butyrate Gas Separation Membranes.U.S. Patent 5,096,468.

Sabde, A. D., Trivedi, M., Ramachandhran, V., Hanra, M. and Misra, B. 1997. Casting and characterization of cellulose acetate butyrate based UF membranes. *Desalination,* 114**,** 223-232.

Scholes, C. A., Stevens, G. W. and Kentish, S. E. 2012. Membrane gas separation applications in natural gas processing. *Fuel,* 96**,** 15-28.

Shekhawat, D. 2003. A review of carbon dioxide selective membranes. *US department of energy***,** 9-11.

Suttiwijitpukdee, N., Sato, H., Zhang, J., Hashimoto, T. and Ozaki, Y. 2011. Intermolecular interactions and crystallization behaviors of biodegradable polymer blends between poly (3-hydroxybutyrate) and cellulose acetate butyrate studied by DSC, FT-IR, and WAXD. *Polymer*, 52, 461-471.

Thomas, R., Guillen-Burrieza, E. and Arafat, H. A. 2014. Pore structure control of PVDF membranes using a 2-stage coagulation bath phase inversion process for application in membrane distillation (MD). *Journal of Membrane Science,* 452**,** 470-480.

Tiraferri, A., Yip, N. Y., Phillip, W. A., Schiffman, J. D. and Elimelech, M. 2011. Relating performance of thin-film composite forward osmosis membranes to support layer formation and structure. *Journal of Membrane Science,* 367**,** 340-352.

Wan, Y., Creber, K. A., Peppley, B. and Bui, V. T. 2004. Structure and ionic conductivity of a series of di-o-butyrylchitosan membranes. *Journal of applied polymer science,* 94, 2309-2323.

Wan, Y., Creber, K. A. M., Peppley, B. and Bui, V. T. 2003. Ionic conductivity of chitosan membranes. *Polymer,* 44**,** 1057-1065.

Wang, Y., Lau, W. W. and Sourirajan, S. 1994. Effects of membrane-making conditions and shrinkage treatment on morphology and performance of cellulose acetate butyrate membranes. *Separation science and technology,* 29**,** 1689-1704.

Xia, S. and Ni, M. 2015. Preparation of poly (vinylidene fluoride) membranes with graphene oxide addition for natural organic matter removal. *Journal of Membrane Science,* 473**,** 54-62.

Xin, Q., Gao, Y., Wu, X., Li, C., Liu, T., Shi, Y., Li, Y., Jiang, Z., Wu, H. and Cao, X. 2015. Incorporating one-dimensional aminated titania nanotubes into sulfonated poly (ether ether ketone) membrane to construct CO_2-facilitated transport pathways for enhanced CO_2 separation. *Journal of Membrane Science,* 488**,** 13-29.

Xu, Z., Zhang, J., Shan, M., Li, Y., Li, B., Niu, J., Zhou, B. and Qian, X. 2014. Organosilane-functionalized graphene oxide for enhanced antifouling and mechanical properties of polyvinylidene fluoride ultrafiltration membranes. *Journal of Membrane Science,* 458**,** 1-13.

Yang, H., Xu, Z., Fan, M., Gupta, R., Slimane, R. B., Bland, A. E. and Wright, I. 2008. Progress in carbon dioxide separation and capture: A review. *Journal of Environmental Sciences,* 20**,** 14-27.

Yang, Y. and Wang, P. 2006. Preparation and characterizations of a new PS/TiO_2 hybrid membranes by sol–gel process. *Polymer,* 47**,** 2683-2688.

Yave, W., Car, A., Funari, S. S., Nunes, S. P. and Peinemann, K. V. 2009. CO_2-philic polymer membrane with extremely high separation performance. *Macromolecules,* 43**,** 326-333.

Zha, S., Yu, J., Zhang, G., Liu, N. and Lee, R. 2015. Polyethersulfone (PES)/cellulose acetate butyrate (CAB) composite hollow fiber membranes for BTEX separation from produced water. *RSC Advances,* 5**,** 105692-105698.

Zhu, W. P., Sun, S. P., Gao, J., Fu, F. J. and Chung, T. S. 2014. Dual-layer polybenzimidazole/polyethersulfone (PBI/PES) nanofiltration (NF) hollow fiber membranes for heavy metals removal from wastewater. *Journal of Membrane Science,* 456**,** 117-127.